Geomorphology 432 (2023) 108692

Contents lists available at ScienceDirect

Geomorphology

journal homepage: www.journals.elsevier.com/geomorphology

Riverbank erosion and char stability along the fluvial-to-tidal transition zone in the Lower Meghna River and Tentulia Channel in the Ganges-Brahmaputra-Meghna Delta, Bangladesh

Leslie A. Valentine [a,*], Carol A. Wilson [b,c]

[a] Department of Geosciences, Middle Tennessee State University, Murfreesboro, TN, USA
[b] Department of Geology and Geophysics, Louisiana State University, Baton Rouge, LA, USA
[c] Coastal Studies Institute, Baton Rouge, LA, USA

ARTICLE INFO

Keywords:
Fluvial-to-tidal transition zone
Riverbank erosion
Relative sea-level rise
GBM delta

ABSTRACT

The Ganges-Brahmaputra-Meghna (GBM) delta has been named one of the world's most vulnerable sinking deltas. It is also one of the most dynamic deltas, with the world's highest sediment discharge and third highest water discharge, with semi-diurnal mesoscale (2–4 m) tides. The high fluvial discharge and significant tidal velocities (1–2 m/s) create an expansive fluvial-to-tidal transition zone (FTTZ) along the entire Lower Meghna River (LMR). Within this FTTZ, tidally elongated channel bars, locally called 'chars', rapidly evolve due to the high sediment and water discharges. Chars along the LMR have a total population exceeding 5 million people; thus, evaluating the interactions of fluvial and tidal processes along the FTTZ is crucial to understanding vulnerability among char communities with respect to flooding and sea-level rise. Here, we utilize a multi-faceted approach to assess the geomorphology, sedimentology, and hydrology of three chars longitudinally spaced within the LMR and one of its distributaries – the Tentulia Channel. Decadal land change analyses revealed that the FTTZ along the upper LMR and Tentulia Channel has been gaining land at a rate of 4.7 km2/yr, with erosion being most prevalent upstream and most accretion occurring within 50 km of the coast. Almost all the stratigraphic profiles show fine and/or medium sands at depth (0.5–2 m), implying that the three chars are similarly susceptible to erosion by tidal currents and high river discharge. Thus, we attribute the increased stability of chars in the downstream direction to increased tidal influence rather than sedimentology. Land elevation and water level surveys reveal that elevation relative to sea level decreases as the distance to the mouth of the LMR decreases: from 4.05 m (130 km from the mouth), to 2.56 m (100 km from the mouth), and 1.85 m (70 km from the mouth). By incorporating local water level data with the elevation surveys, we conclude that fluvial, namely monsoonal, processes control the geomorphology of the chars near the confluence of the LMR and the head of Tentulia Channel. The shift between fluvial-dominated and tidal-dominated regions of the FTTZ occurs just downstream of Char 3 (~70 km from the LMR mouth). Therefore, char communities near the LMR confluence are most vulnerable to riverbank erosion and flooding associated with the monsoon season, and chars proximal to the coast are most vulnerable to erosion and flooding related to storm surges and relative sea-level rise.

1. Introduction

The Ganges-Brahmaputra-Meghna (GBM) delta spans ~150,000 km^2 and is home to >200 million people in Bangladesh and West Bengal, India. It is the world's largest delta in terms of sediment load, with 1 billion tons of sediment discharging into the Bay of Bengal every year and the 3rd largest in terms of average water discharge (~38,000 m^3/s). Every year, millions of people in the delta are negatively affected by riverbank erosion, especially during the monsoon season (June-mid October) when the Ganges, Brahmaputra/Jamuna, and Meghna river basins receive 80 % of their annual rainfall, causing the rivers to swell. Of the 200 million people that live in the GBM delta, approximately 2–3

Abbreviations: GBM, Ganges-Brahmaputra-Meghna; LMR, Lower Meghna River; FTTZ, fluvial-to-tidal transition zone.

* Corresponding author at: Department of Geosciences, Middle Tennessee State University, Murfreesboro, TN 37132, USA.
E-mail address: leslie.valentine@mtsu.edu (L.A. Valentine).

https://doi.org/10.1016/j.geomorph.2023.108692
Received 19 July 2022; Received in revised form 31 March 2023; Accepted 2 April 2023
Available online 11 April 2023

million (~1–2 %) reside on chars along the Lower Meghna River (LMR), making them some of the most vulnerable populations (Sarker et al., 2003). In Bangladesh, the word 'char' or 'charland' is the general term to describe river bars; they can be attached or unattached to the mainland and exhibit various stages of vegetation and human inhabitation. Char age, size, and geologic properties (sedimentology and stratigraphy) depends upon the sedimentological and hydrological conditions of the respective river channels.

Of the three rivers that form the GBM delta, the Ganges and Meghna Rivers have meandering planforms, while the Brahmaputra-Jamuna River is braided (Fig. 1). The Brahmaputra-Jamuna River is the greatest of the three rivers in terms of slope (7.5×10^{-5}), median bed grain size (220 μm; fine sand), sediment discharge (590 Mt./a), and average annual water discharge (20,200 m^3/s) (Sarker et al., 2003). By comparison, the Ganges and Meghna Rivers both have lower slopes (5.0×10^{-5} for both) and similar median bed grain sizes of 150 and 140 μm (fine sands) (Sarker et al., 2003). However, the Ganges has an average annual discharge of 11,300 m^3/s and transports 550 Mt. of sediment every year, while the Meghna River has an average annual discharge of 4600 m^3/s and transports only 13 Mt. of sediments annually (Sarker et al., 2003).

While chars are most prolific in the braided Brahmaputra-Jamuna River upstream of the Padma River confluence (>200 chars), the high discharge and relatively larger grain size lead to riverbank instability and erosion, resulting in an average char lifespan of only 5 years (Ashworth et al., 2000; Best et al., 2003, 2007; Khan and Islam, 2003; Ruknul Ferdous et al., 2018). Alternatively, chars in the lower-gradient, Ganges and Meghna meandering rivers upstream of their respective confluences (the Padma River and Lower Meghna River confluences) are relatively more stable, having average life-cycles ≥10 years (Sarker et al., 2003; Oberhagemann et al., 2021). Ultimately, the Ganges and Brahmaputra-Jamuna Rivers coalesce to form the Padma River, which continues flowing southeast (Fig. 1). It is within the ~110 km Padma River that a change in the hydrologic regime begins as fluvial processes are impacted by tidal forcings, with the inland tidal limit located ~60 km downstream of the Padma confluence (~215 km from river mouth; shown in Fig. 1). The Padma continues flowing downstream, coalescing with the Upper Meghna River to form the Lower Meghna River (LMR), which eventually bifurcates into 3 main distributary channels that discharge into the Bay of Bengal. From the inland tidal limit in the Padma River to the Bay of Bengal, the GBM delta is simultaneously affected by varying fluvial and tidal forcings, creating a complex depositional environment commonly referred to as the fluvial to marine transition zone or the fluvial to tidal transition zone (FTTZ) zone, as it will be referred to in this study.

Previous studies of the FTTZ zone in meso- to macro-tidal deltas conclude that areas of high lateral migration (i.e. riverbank erosion) and sinuosity are driven by mass extraction of sediments, with a significant fining downstream (Dalrymple and Choi, 2007; Bomer et al., 2019). Mass extraction of sediments occurs when the carrying capacity is reduced, causing coarser grains to fall out of suspension, oftentimes linked to either a change in slope or opposing tidal current forces. In the case of the meso-tidal and macro-tidal scale deltas, mass extraction occurs at the upstream limit of the tides (opposing forces) as well as the upstream limit of the backwater zone (decrease in slope). In the GBM delta, it is difficult to constrain the regions of mass extraction as tidal limits and backwater zones are non-stationary, both being influenced by seasonal fluctuations in fluvial discharge, monsoonal wind patterns, and cyclones and associated storm surges (Barua, 1990; Alam, 1996; Elahi et al., 2020). Thus, with their proximity to the coast, chars are not only vulnerable to riverbank erosion from high water discharge during the monsoon but also to sea-level rise (SLR) and cyclones. Additionally, the backwater extent in the GBM delta is only moderately documented due

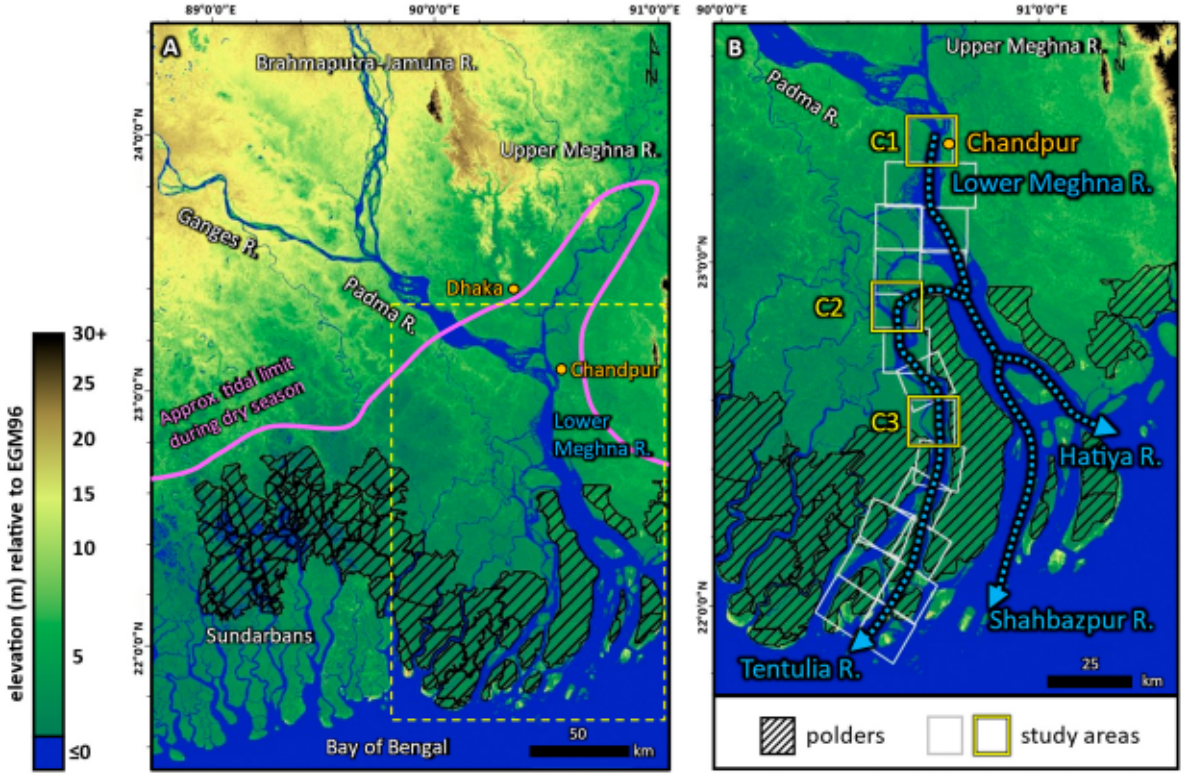

Fig. 1. (A) Coastal DEM of the Ganges-Brahmaputra-Meghna Delta in Bangladesh. The study area (outlined by yellow dashes in A) is located along the Lower Meghna River and the Tentulia River, an offshoot of the Lower Meghna River. (B) Three detailed study areas and their chars are highlighted in yellow (C1, C2, C3), and the light gray boxes are additional study sites of equal areal extent (225 km^2) used to assess general erosion and accretion along the fluvio-tidal transition zone (FTTZ) within the Lower Meghna River. Approximal tidal limit from FAO, 1985. (For interpretation of the references to colour in this figure legend, the reader is referred to the web version of this article.)

to a paucity of available bathymetric data (Bricheno et al., 2016; Bomer et al., 2019; Gugliotta and Saito, 2019). Gaining a better understanding of mass extraction and sedimentation patterns in the Lower Meghna River has significant implications for riverbank erosion within the FTTZ, but to date, previous studies have only been 2-dimensional (x,y direction).

Assessments of flood risk across the FTTZ within the GBM delta have been considerably limited by outdated, low-resolution elevation data as the last large-scale survey was completed over 20 years ago (though recently corrected by Kulp and Strauss, 2019, original SRTM data was collected in 2000). In a delta that discharges over 1 billion tons of sediment every year, the amount of accretion and erosion that can occur in 20 years is immense. To quantify the amount and variability of riverbank erosion in the relatively understudied Tentulia River, this study provides 3-dimensional (lateral, x and y, and vertical, z, measurements) geological analyses of char stability along the FTTZ in the GBM delta. The main thrust of our study is to assess char stability and flood risk in terms of riverbank erosion and land surface elevations for the FTTZ of the Lower Meghna River. Our study focuses on 3 regions longitudinally spaced along the Lower Meghna River and Tentulia River using a multifaceted approach that enlists: (1) remote sensing data to document riverbank erosion on a decadal scale over the past 40 years, (2) shallow (5 m) sediment cores in areas of active erosion and accretion to incorporate sedimentology into the riverbank erosion analysis, and (3) new, localized land and water elevation surveys to assess future riverbank erosion and flood risk.

2. Study area

Three regions longitudinally spaced within the FTTZ of the Lower Meghna River (LMR) and the char islands contained within are the focus of this study, hereafter named C1, C2, and C3 (Fig. 1). Most riverbank erosion, especially in the upstream reaches of the FTTZ (i.e., near C1) occurs when fluvial discharge increases during the monsoon season every year, with maximum monthly peak discharges occurring from July to October (Barua, 1990; Ahmed and Louters, 1997; Kale, 2003; Sokolewicz et al., 2008). The Padma River (Ganges R. Brahmaputra R., Fig. 1), which is the main source of water and sediment for the LMR, has an annual mean flow of 30,000 m^3/s with a bankfull flow of ~75,000 m^3/s (Neill et al., 2013). A bankfull flow is the maximum discharge a channel can carry without overflowing, and the Padma discharge can exceed 100,000 m^3/s during the monsoon season, which puts it well over the bankfull threshold, effectively flooding adjacent lands. During bankfull flow, average river velocities at the Padma Bridge (~43 km upstream of the confluence of the Padma and Meghna Rivers) range from 1.2 to 1.6 m/s, with maximum vertically-averaged velocities ranging from 2.1 to 2.7 m/s (Ahmed and Louters, 1997). The Upper Meghna River coalesces with the Padma to form the LMR, contributing an average flood discharge of 13,700 m^3/s, with modeled current velocities exceeding 1.5 m/s during the wet season (Alam, 2014; Syed et al., 2018).

Approximately 30 km downstream of its confluence, the LMR bifurcates, sending 7 20 % of its flow to the western distributary, the Tentulia Channel (C2; Fig. 1). The mainstem LMR continues south for ~40 km before splitting into the central Shahbazpur and eastern Hatia distributary channels near the coastline. Large chars (100 km^2) are present along the central and eastern Meghna Estuary, while chars along the Tentulia River are considerably smaller (Fig. 1). Chars along the upper LMR and Tentulia Channel were selected for analyses because the average population density of these areas is 1000 persons/km^2, while chars in the Shahbazpur and Hatia Channels typically have population densities of 500 1000 persons/km^2 (Becker et al., 2020). Data from 1996 to 1998 show that the Tentulia River discharge varies from ~3000 m^3/s during the dry season to ~15,000 m^3/s during the monsoon an increase of 400 % (Ahmed and Louters, 1997). Approximately ~20 km downstream of C2 (and ~ 10 km north of C3), measured discharge data from 1990 to 1992 recorded maximum velocities in the Tentulia Channel ranging from 1.1 to 1.4 m/s during spring tides in the monsoon season (Ahmed and Louters, 1997). These flow velocities are similar to other fluvio-tidal to tidal-dominated estuaries like Amazon, Fly, and Mekong river deltas, in which maximum flow velocities exceed 1.5 2 m/s in the estuaries (Harris et al., 2004; Barros et al., 2011; Nowacki et al., 2015).

3. Methods

3.1. Shoreline analyses and geometric calculations

Net land change (erosion vs accretion) was assessed for the FTTZ that encompasses the three study regions and their chars, from the upper section of the Lower Meghna River (LMR) to the Tentulia River (an offshoot channel of the LMR) to the Bay of Bengal (Fig. 1). In total, this comprised 19 study boxes of equal areal extent (225 km^2), including the 3 specific study chars and their respective buffer zones (C1, C2, C3). Landsat imagery (resolution 30 m) was downloaded from Earth Explorer and used for the analyses for the years 1978, 1991, 2000, 2010, and 2019. The Landsat images were cross-referenced with tide data from Bangladesh Water and Development Board (BWDB) and Bangladesh Inland Water Transport Authority (BIWTA) to ensure all images were representative of low tide stages this is important as the southern study areas, C2 and C3, experience tidal ranges 2 m during spring high tides. The Tabulate Area tool in ArcMap was used for binary classifications, based on the pixel values for each image (water will appear black and land white in short-wave infrared images). After determining land and water classification for each pixel in the study box, the values for the two classes (land and water) were summed and expressed in terms of Water (km^2) and Land (km^2) . By comparing the Land (km^2) values for different years, net land change was calculated, where negative values represent land loss and positive values represent land gain. The binary classification analyses provide a general idea of sedimentation within the fluvio-tidal regime, and they also aid in determining if small-scale patterns observed at the three study chars (C1, C2, C3) are anomalous or representative of the entire study region.

Detailed accretion and erosion of the three study chars (C1, C2, C3) were analyzed using the same historical imagery as the binary classifications. For the three study sites, study boxes of equal areal extent (225 km^2) were created from the centermost point of the chars; similar to above, having equal areal extent allows for standardized calculations given different dimensions of the chars going from upstream to downstream. Within each 225 km^2 box, waterbodies were manually traced in ArcMap using the polygon feature, and the Calculate Geometry tool was used to calculate the areas of the waterbodies for each year. The area of land within each box was calculated by subtracting the waterbody areas from the total area (225 km^2). Erosion and accretion measurements for each time interval (1978 to 1991, 1991 to 2001, 2001 to 2010, and 2010 to 2019) were obtained by using the Union tool to classify land change between the two respective years. Erosion rates for each time interval along with the overall erosion rates for each site were then calculated. Manually digitizing shorelines is more accurate than binary classification, especially in the lower-resolution Landsat 4 and 5 images (30 m resolution), as image noise (isolated pixels) corrections can be made.

3.2. Coring and sedimentological analyses

Aerial imagery analyses identified specific areas on all 3 chars that had recently experienced erosion or accretion, and sediment cores were taken in these areas to determine if there were significant differences in sedimentology between erosional and accretional areas. Additionally, sediment cores were collected along longitudinal and lateral transects on the chars to assess spatial variability in sedimentology. The number of cores collected per study site are as follows: 3 cores on Char 1 (C1), 5

cores on Char 2 (C2), and 4 cores on Char 3 (C3), for a total of 12 cores. Auger cores were extracted by hand using a 5.08-cm diameter Edelman combination auger to an average depth of 2.9 m, subsampled in the field at 20 cm intervals. Compaction during auger coring was minimal. All core samples were then shipped and analyzed at Louisiana State University Sedimentology lab for bulk density, organic content via loss-on-ignition, and grain size using the same methods as Valentine et al. (2021).

Erodibility of Sediments.

Erodibility of chars was quantified by calculating and comparing the bed shear stresses and critical erosional shear stresses of sediment intervals (~20 cm) of each collected core using the Shields diagram. On the diagram, the Boundary Reynold s number (R_{e*}) is plotted on the x-axis and the Critical Shields Stress ($_c$) is plotted on the y-axis. To plot the samples on a Shield s diagram, the following equations were used:

$$* \quad \left(- \right)$$

$$*$$

$$\frac{\qquad}{\left(\qquad \right)}$$

$$* \quad \frac{*}{\qquad}$$

where U_* is bed shear velocity (m/s), D is the median grain size (m), h is the average channel depth (m), U(h) is the current speed (m/s) at depth (h), $_0$ is the bed shear stress (N/m^2), $_s$ is the sediment density (kg/m^3), $_f$ is the fluid density (kg/m^3), g is the acceleration due to gravity (m/s^2), and v is the kinematic viscosity of water (m^2/s). The median grain sizes were calculated using the methods listed previously and the average channel depths and current speeds are from observed and modeled data (Ahmed and Louters, 1997; Bricheno et al., 2016; Hale et al., 2019). We assume that the erosion is critical to the sand and cohesion may be negligible as discussed below in Section 4.4 Sedimentological Analyses and Section 5.1.2 Sedimentology and Flow Regimes Implications for Char Stability in the Downstream FTTZ .

3.3. Surface and water elevation data

Elevation transects were measured (relative to elevation datum EGM 96) using an RTK (real-time kinematic) GPS system with a Leica GS16 base antenna and GS18T rover. Kriging contour maps were created from the measured GPS points within all 3 study areas chars (C1, C2, C3) using Surfer®17.

For each study char, multiple GPS surveys were conducted typically at erosional and accretionary areas; an average of 450 GPS points per survey was measured. Once the points were measured, elevation and stratigraphic profiles were created using kriging interpolation in Surfer 17® and Adobe Illustrator. Studies have shown kriging is useful in small areas as it distributes weight based on statistical autocorrelation, and the result is a smoother grid/3D surface than that of other commonly used interpolation methods (e.g., nearest neighbor or bilinear (Arun, 2013)). To obtain the relative water surface elevations, HOBO® pressure sensors were deployed at locations that received tidal input. Then, water surface elevations (relative to EGM 96) were measured with the Leica GPS system from the shoreline, noting the time. Thus, the water surface measurements taken with the Leica GNSS system were cross-referenced with the relative water surface elevations (HOBO®) to calculate absolute water surface levels at different tide stages relative to EGM 96.

Elevation data collected in 2019 was then compared to elevation data from CoastalDEM90 v2.1, a DEM derived from Shuttle Radar Topography Mission (SRTM; February 2000) data. CoastalDEM90 v2.1 has a resolution ~90 m, with significant improvements (from CoastalDEM 1.1 and other publicly available DEMs) in vertical bias due to vegetation, artificial structures, and noise, especially in areas with maximum elevations of 5 m above MSL (Kulp and Strauss, 2019, 2021). In ArcMap, the XYZ points collected in 2019 were added as a layer on top of the CoastalDEM from 2000, and polygons were created for each individual survey site. The polygons were created by outlining the survey grids, excluding XYZ points that were water (elevations at or below 0 m) in the CoastalDEM. Then, the Zonal Statistics tool was used to calculate the mean elevations for each survey site, using the polygons and DEM as the inputs. As the 2019 survey sites only cover a small portion of the chars, average char elevations were calculated using both the CoastalDEM data and the 2019 measurements.

4. Results

4.1. Geospatial analyses binary calculations for the Lower Meghna and Tentulia Rivers

The binary classification geospatial analyses provided an overall trend of the sedimentation processes within the FTTZ of the LMR and Tentulia River (offshoot channel of the LMR). While the calculated values are presented as total area of land (km^2), the Tabulate Area tool in ArcMap was used, which can only calculate geodetic distances as opposed to planimetric distances. The distortion between the two coordinate systems (WGS 84 Web Mercator and WGS84 UTM Zone 46N) is estimated using the equation: 1/cos(latitude) (Snyder, 1997). All the study areas are within latitudes of 21.9 N and 23.3 N, thus the scale of distortion ranges from 1.08 and 1.09, respectively; that is, the geodetic distance is 1.08 or 1.09 times that of the planar distance (the distance measured on the ground). The distortion is represented as error in Table 1.

Overall, 13 of the 19 areas experienced net accretion from 1978 to 2019, with net land gain ranging from 0.7 to 52.7 km^2, which is a net land change of 0.3 to 23 %, respectively (Fig. 2, Table 1). The average net land gain for the 13 sites was 23.8 km^2 or ~ 11 %. Of the remaining 6 of 19 areas, the net erosion ranged from 3.3 to 38.4 km^2, or 2 to 17 %, respectively (Table 1). Therefore, the average net erosion from 1978 to 2019 for the six sites was 19.5 km^2, which is 20 %. Five of the six sites with net erosion are within 50 km of the confluence of the Padma and Meghna Rivers, with the sixth site being proximal to the Bay of Bengal (Fig. 2).

The period with the greatest net accretion occurred between 1978 and 1991, with 13 sites having a combined accretion of 218.4 km^2, an average gain of 16.8 km^2 (7.5 %) per site. Area D (Table 1) had the highest net accretion during this period, and this area is located on the west bank of the Lower Meghna River, just north to the Tentulia River offshoot. In subsequent periods, this area would experience net erosion of 21.6 km^2 from 1991 to 2010, followed by a land gain of 7.6 km^2 from 2010 to 2019. Area R , which is at the mouth of the Tentulia River experienced net accretion for all periods leading up to 2010 (total net land gain of 28.6 km^2). Then, from 2010 to 2019, over 60 km^2 (~27 %) of the land was eroded. As a whole, the Lower Meghna and Tentulia Rivers are accreting, having experienced a net land gain of 192.7 km^2 from 1978 to 2019, with most accretion occurring within 50 km of the Bay of Bengal in the Tentulia Channel (Fig. 2).

4.2. Geospatial analyses detailed calculations for three chars (C1, C2, and C3)

More detailed land change analyses were conducted for the 3 study chars C1, C2, and C3 (A , H , and K squares); C1 and C2 experienced net erosion, while C3 experienced net accretion. This is in agreement with the binary classifications for C1 and C2; as noted in Table 1, image noise skewed the binary measurements for total land for site C3 (square K) for 1978, thus the two methods cannot be accurately compared for C3. The manual shoreline classifications allow for analyses

Table 1
The 19 different study boxes with their respective River Id, Square Id, and Land change calculations. The red values indicate net erosion from 1978 to 2019. *For "A", which is where site C1 is located, the estimate for total land for 2001 is inaccurate due to cloud cover. For "K", where site C3 is located, the estimate for total land in 1978 is inaccurate due to image noise. Additionally, 2 separate Landsat images were stitched together for analyses, which led to inaccurate classification due to discrepancies between pixel values. Further detailed shoreline analyses reveal the net land gain to be closer to 2.2 km^2 (shown in Fig. 3 & Table 2).

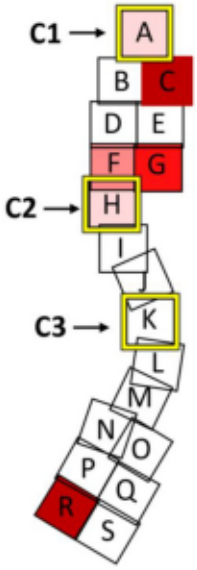

Total Land (km^2) along Lower Meghna and Tentulia Rivers

River ID	Square ID	1978	1991	2001	2010	2019	Net land gain (km^2) from 1978 to 2019
Meghna	A	156.0	150.7	163.3*	135.8	152.7	-3.3 ± 0.2
Meghna	B	145.3	156.4	145.5	157.4	187.1	41.9 ± 4.2
Meghna	C	197.8	195.5	183.0	164.0	159.4	-38.4 ± 3.3
Meghna	D	140.1	192.6	183.4	171.0	178.6	38.5 ± 3.5
Meghna	E	118.3	102.2	111.0	136.2	121.6	3.3 ± 0.3
Meghna	F	181.0	187.8	186.2	170.4	167.4	-13.6 ± 1.2
Meghna	G	104.9	123.9	108.2	101.9	79.2	-25.7 ± 2.0
Tentulia	H	169.3	177.6	172.9	163.3	165.0	-4.4 ± 0.1
Tentulia	I	154.0	177.9	177.9	176.3	166.9	12.9 ± 1.2
Tentulia	J	160.1	177.0	170.7	176.4	172.9	12.8 ± 1.6
Tentulia	K	144.9*	174.3	160.0	164.7	166.6	2.2 ± 2.0
Tentulia	L	136.0	136.0	144.7	156.5	156.4	20.4 ± 2.5
Tentulia	M	114.6	134.1	141.7	144.5	153.7	39.1 ± 3.5
Tentulia	N	158.4	152.3	153.4	152.7	159.1	0.7 ± 0.1
Tentulia	O	165.1	178.6	186.5	191.3	189.0	23.9 ± 2.7
Tentulia	P	136.3	142.2	151.8	160.4	165.2	28.9 ± 3.2
Tentulia	Q	107.0	126.1	137.6	149.8	159.7	52.7 ± 5.6
Tentulia	R	118.8	135.4	144.7	147.4	87.2	-31.7 ± 2.5
Tentulia	S	40.9	46.3	56.3	66.3	73.2	32.3 ± 3.2

highlighting the extent and location of accretion and erosion for each time interval. For example, while C1 had net land gain of −3.3 km^2 from 1978 to 2019, 58 km^2 of land accreted during this time and 61.2 km^2 was eroded; this means ~30 % of the land within the site experienced land change (erosion and/or accretion). Site C2 had the most lateral mobility, with 82.6 km^2 of accretion and 84.9 km^2 of erosion from 1978 to 2019, with ~48 % of the area experiencing erosion and/or accretion from 1978 to 2019. Site C3, while being the only site with net accretion, experienced the least amount of land change, although it was still substantial: the total amount of accretion was 38.2 km^2 and the total amount of erosion was 36.0 km^2, therefore ~25 % of the site underwent land change.

The manually digitized shorelines allowed us to identify areas of the chars (within the 225 km^2) that have been actively accreting or eroding, which is important for population centers and environmentally-forced migration. For Char 1 (C1), just downstream of the confluence of the Padma and Meghna Rivers, the north and north-eastern sides of the char are actively eroding, while the southern end of the char is actively accreting (Fig. 3). Char 2 (C2) is located near the head of the Tentulia River, which is an offshoot of the Lower Meghna River. At C2, most of the erosion is lateral – along the western and eastern sides, while most accretion is occurring along the southern and northeastern ends of the char (Fig. 3). For Char 3 (C3), which is the southernmost char located in the Tentulia River, both the northern and southern boundaries of the char are eroding, while the central western section is accreting (Fig. 3).

4.3. Elevation data

Elevation surveys were conducted at each char proximal to eroding and accreting shorelines; as a general trend, average char elevation decreased with proximity to the Bay of Bengal. However, the elevation surveys only cover a small area of the chars; thus, the survey data were combined with the CoastalDEM90 data to calculate average char elevations. For C1, the survey elevation data collected in 2019 was used to calculate the average char elevation (4.1 m), as that area underwent a lot of morphological change between 2000 and 2019, with nearly 40 % of the 2019 land area accreting after 2000 (see Fig. 3; Fig. 4). Site C2, located 50 km downstream of C1, was more stable, and average char elevations of both datasets were ~2.5 m (Fig. 4). Site C3 was the most laterally stable char, with close agreement between average elevations of survey areas from the stable interiors, sites C3-N and C3-S (Table 3). As much of the char was stable throughout 2000–2019, the average char elevation (~2.0 m) was calculated from the CoastalDEM and elevation measurements from this study (Fig. 4). Overall, the regional land surface slope along the Lower Meghna River is ~2.1 × 10^{-5} (Fig. 4).

While average elevation decreases with proximity to the coast when assessing the Lower Meghna River as a whole, age appears to correlate with elevation on a smaller scale across individual chars. That is, char islands are a composite (almost patch-work quilt) of younger and older sections (shown in Fig. 3), with the older sections measuring higher in elevation, and younger sections measuring lower in elevation (Table 3). Furthermore, older areas that are close to eroding shorelines appear to be higher in elevation than newly accreted sections of chars. Interestingly, the elevation surveys also elucidated average elevations along erosional shorelines were always greater than elevations along accretionary shorelines on the same char, even if the erosional shoreline was further downstream (Table 3). For example, 3 elevation surveys were conducted for C3, the southernmost char; the northern and southern shorelines of C3 were both erosional, while the western shoreline was accretionary (Fig. 3). The southern shoreline had the highest average elevation at 2.3 ± 0.1 m (with a maximum recorded height of 2.9 m), followed by the northern shoreline (average elevation of 2.0 ± 0.1 m) and lastly the western shoreline (average elevation of 1.4 ± 0.3 m) (Table 3). Fig. 3 shows that the southern and northern regions of the char pre-date 1978, however the western region of the char developed between 1978 and 2019.

In addition to land surface elevation data, water surface elevation data were collected at all 3 sites. At Site C2, located near the head of the

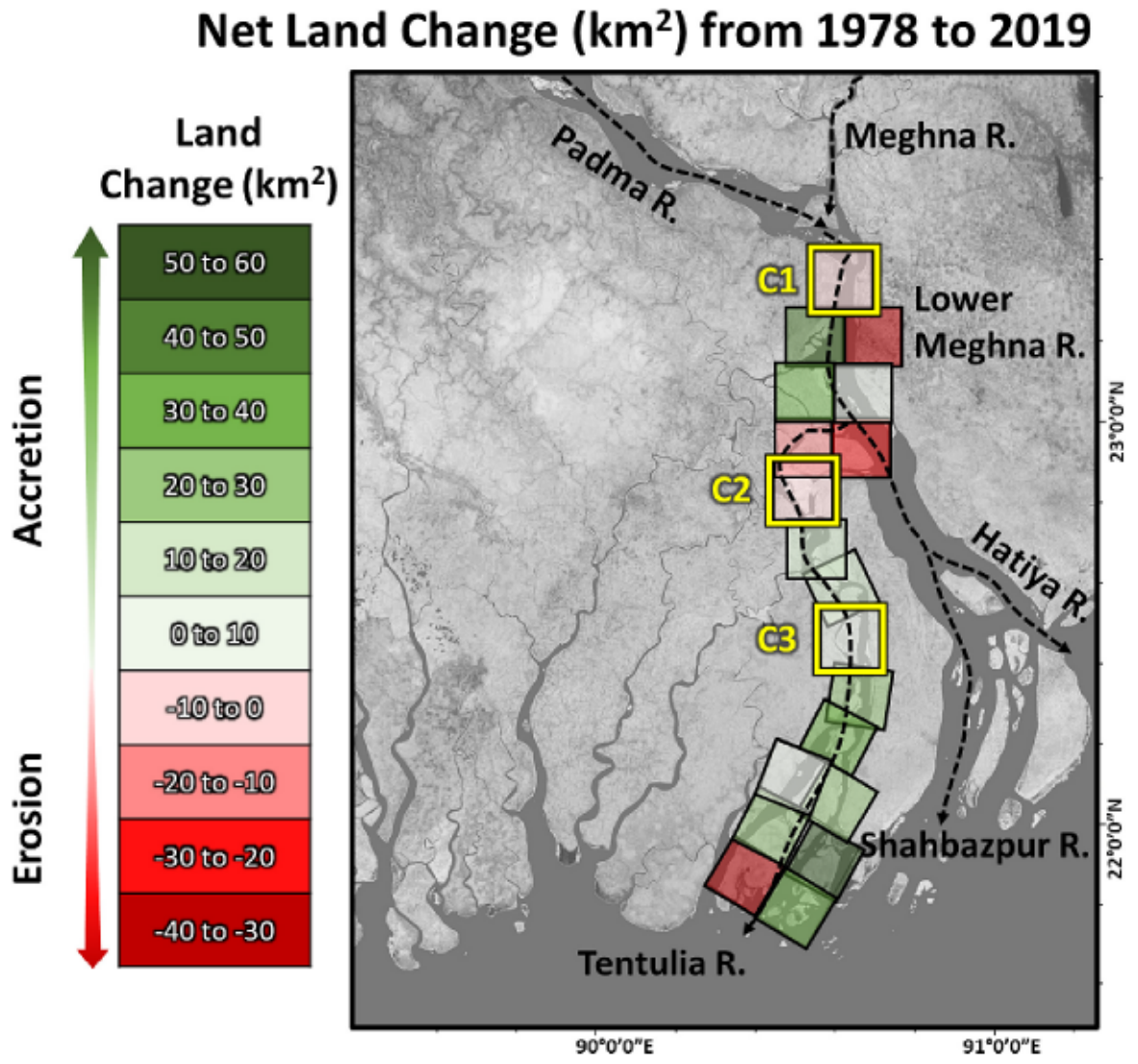

Fig. 2. Net land change (km^2) from 1978 to 2019, for the upper reach of the Lower Meghna and Tentulia Rivers. These analyses are based on binary classifications (land vs water) of Landsat images. The timestamps of the images were cross-referenced with tide tables to ensure the images are reflective of low tide stages, which is important as the southern sites experience tidal ranges >2 m, especially during spring high tides. Each square is 225 km^2, and the respective C sites are outlined in yellow. Warmer colors represent net erosion, while cooler colors represent net accretion. Overall, there was net accretion, especially in the Tentulia Channel. C1 and C2 experienced net erosion of −3.3 km^2 and −4.4 km^2, respectively. C3 experienced net accretion of 2.2 km^2. While the binary calculations are not as accurate as the manually-derived calculations (shown in Fig. 3, discussed in the text), the binary classification is a relatively quick way to assess the net erosion or accretion of an area and gives an idea of the sediment balance throughout the fluvio-tidal regime of the GBM delta. (For interpretation of the references to colour in this figure legend, the reader is referred to the web version of this article.)

Tentulia Channel, a HOBO pressure sensor was deployed in March 2018 and recovered in April 2019, providing long-term (1 year; 30-min interval) water elevation data. The MSL (rel to EGM 96) for Site C2 is 1.63 m, with a mean tidal range of 1.45 m (Figs. 4, 5). The data shows clear tidal signals as well as a monsoonal signal. The increased water elevations from the monsoon peaked in August 2018, with a maximum water level of ~3.5 m, but the monthly mean high water level during August was ~2.1 m, approximately 0.5 m higher than the MSL (Fig. 5). February experienced the lowest water levels, with a monthly mean high water of ~0.9 m. Long-term water surface data could not be collected for Sites C1 and C3, but short-term water elevation data was compared to predicted water levels (BIWTA tide tables) to interpolate the mean tidal range as well as the MSL for both sites. The MSL for C1 is estimated to be 3.5 m (rel to EGM6) and the tidal range is ~0.6 m; C3 has a much lower MSL of 1.2 m (rel to EGM96) but a much larger tidal range of 1.7 m.

4.4. Sedimentological analyses

Most cores are silt-dominated with fining-upward sequences, with sand content increasing with depth (Figs. 6 and 7A,B,C). The most notable stratigraphic difference between the chars was the decrease in average sand content and median grain size from the fluvial-dominated core in the LMR, C1, to the more tidally influenced cores of the Tentulia Channel, C2 and C3 (Figs. 6 and 7A,C). C1 had an average median grain size of 62.6 μm (very fine sand) and average sand content of 41 %. There was nearly a 50 % reduction in grain size and sand content for C2, which had an average median grain size of 34.5 μm (coarse silt) and sand content of 21 %. C3 had similar values when compared to C2, with an average median grain size of 40.0 μm (coarse silt) and sand content of 26 %. There was no discernible difference in stratigraphy between accretionary and erosional regions on each char, but there were nuanced changes observed with depth for each core location (represented in Fig. 6). For all sites at C1, the average silt content decreased with depth

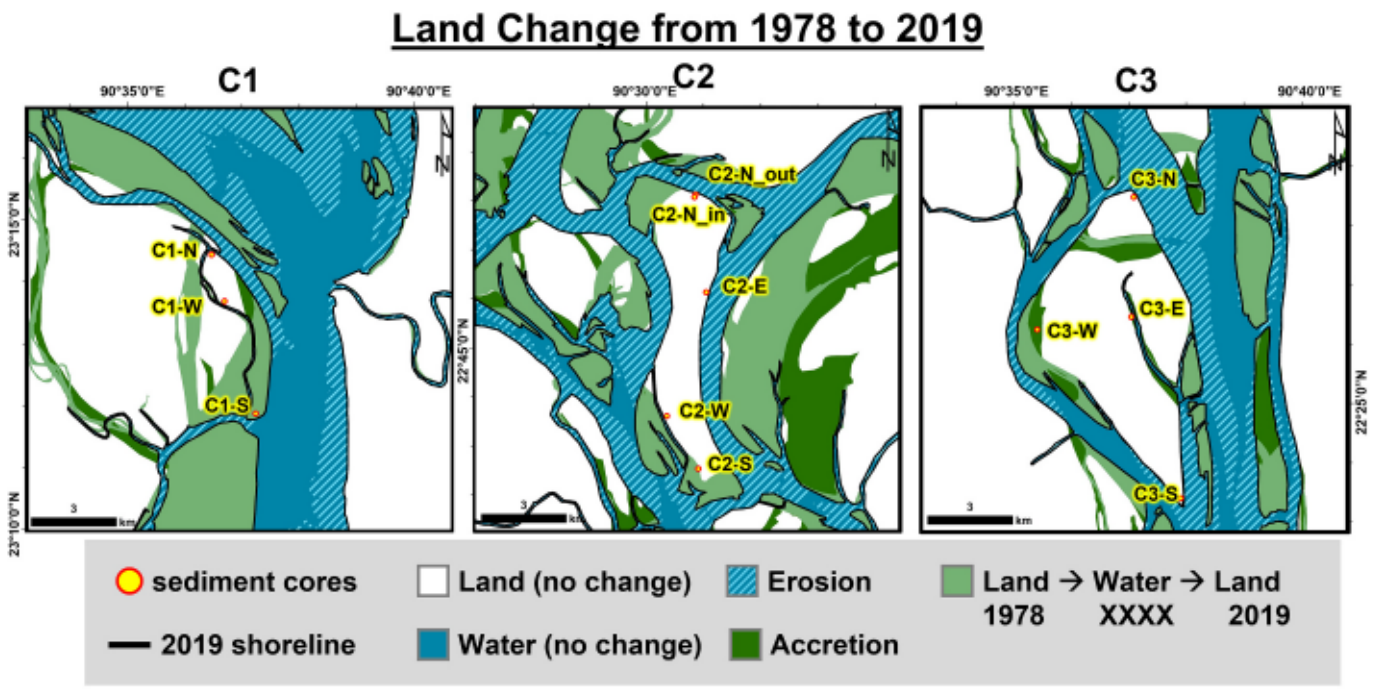

Fig. 3. Detailed land change maps for sites C1, C2, and C3, including core locations for each study char. Comparing endmembers (years 1978 and 2019) does not reflect how much erosion has taken place throughout the years. All 3 sites experienced extensive land change (see Table 2) and erosional rates >2 $km^2\ yr^{-1}$.

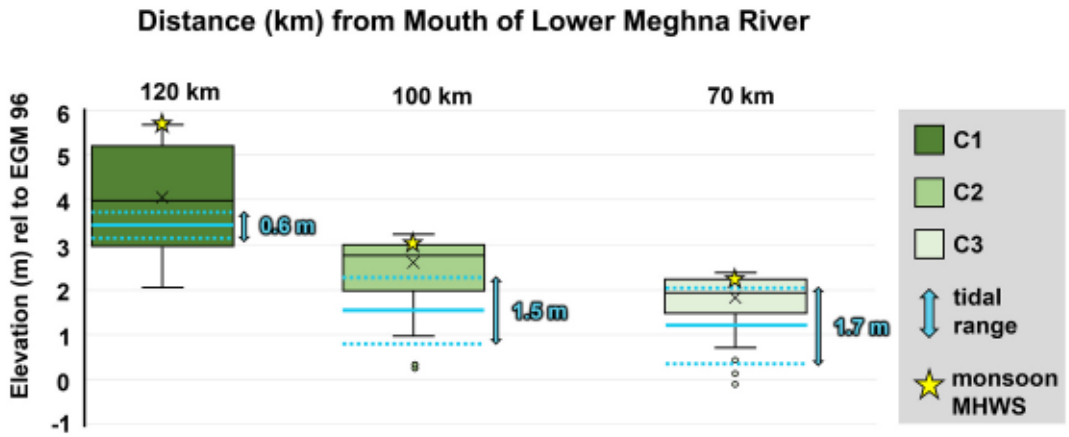

Fig. 4. Average elevations of the three chars and their respective latitudinal locations along the FTTZ in the Lower Meghna River. The overall slope is 2.1×10^{-5}, with average elevations ranging from ~4 m relative to EGM 96 for C1 to ~2 m relative to EGM 96 for C3. The solid blue lines represent the MSL for the 3 chars, and the dotted blue lines represent the tidal ranges. It is evident that platform elevation is dictated by seasonal monsoon high water in the upper (fluvial-dominated) region of the FTTZ, while the platform has aggraded to ~MHW in the lower (tide-dominated) region. (For interpretation of the references to colour in this figure legend, the reader is referred to the web version of this article.)

(70 to 40 %), while the average sand content commensurately increased with depth (22 to 55 %). The southernmost char, C3, also followed a similar pattern with average silt content decreasing from 79 % to 62 % and average sand content increasing from 10 to 33 % with respect to depth. While C2 also followed this trend, the changes are more nuanced. The average silt content decreased only slightly from 74 to 70 % while the average sand content increased from 13 to 22 %. For all cores, clay played a minor role, with average clay content ranging from 4–7 % for C1, 6–12 % for C2, and 7–9 % for C3. While small-scale sedimentary structures are obscured by the sand auger method, structures such as laminations, beds, cross-bedding, and deformation structures (flame structure, dish and pillar) have been observed in trenches and outcrops (Supplemental Fig. S3). Bulk density, LOI, and erodibility data is available in Section 2 of the Supplemental Material.

During the monsoon season, average modeled flow speeds at Chandpur (close to site C1) exceed 2.25 m/s (Uddin et al., 2015); at this speed, all sediments sampled to depths of ~2.5 m are susceptible to erosion as bed shear stresses exceed the critical erosional shear stresses (Fig. 6). During the dry season, average modeled flow speeds are 1.25–1.5 m/s, and all shallow (<5 m) sediments are susceptible to erosion (Fig. 6). For site C2, average modeled flow speeds during the monsoon range from 1.5 to 1.75 m/s (Uddin et al., 2015), leaving all sediments to depths ~3 m vulnerable to erosion (Fig. 6). The average modeled flow speeds for the dry season (1–1.25 m/s; Uddin et al., 2015) also leave all shallow sediments vulnerable to erosion (Fig. 6). Unlike C1 and C2, flow speeds at C3 are greatest during the dry season, with average modeled speeds ranging from 1.25 to 1.5 m/s, and the monsoon average modeled flow speeds for C3 are typically ~1–1.25 m/s. However, the threshold for initiation of motion is still exceeded during both seasons, leaving Char 3 vulnerable to erosion year-round.

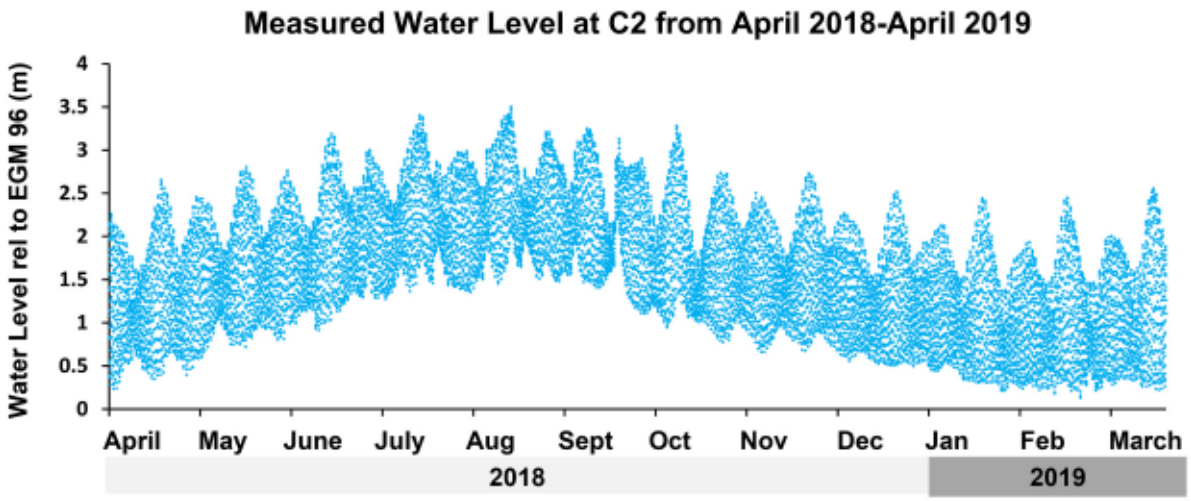

Fig. 5. Water level data for C2 from April 2018–April 2019. The blue dots are individual water levels collected every 30 min. The water level data were converted to the EGM 96 datum by measuring the water surface with the Leica RTK in April 2019. The monsoonal and spring-neap tidal signals are clearly observed in the graph – with higher frequency peaks indicating spring high tides (~ every 2 weeks) and the lower frequency swale indicative of the monsoon high discharge (from May to October 2018). (For interpretation of the references to colour in this figure legend, the reader is referred to the web version of this article.)

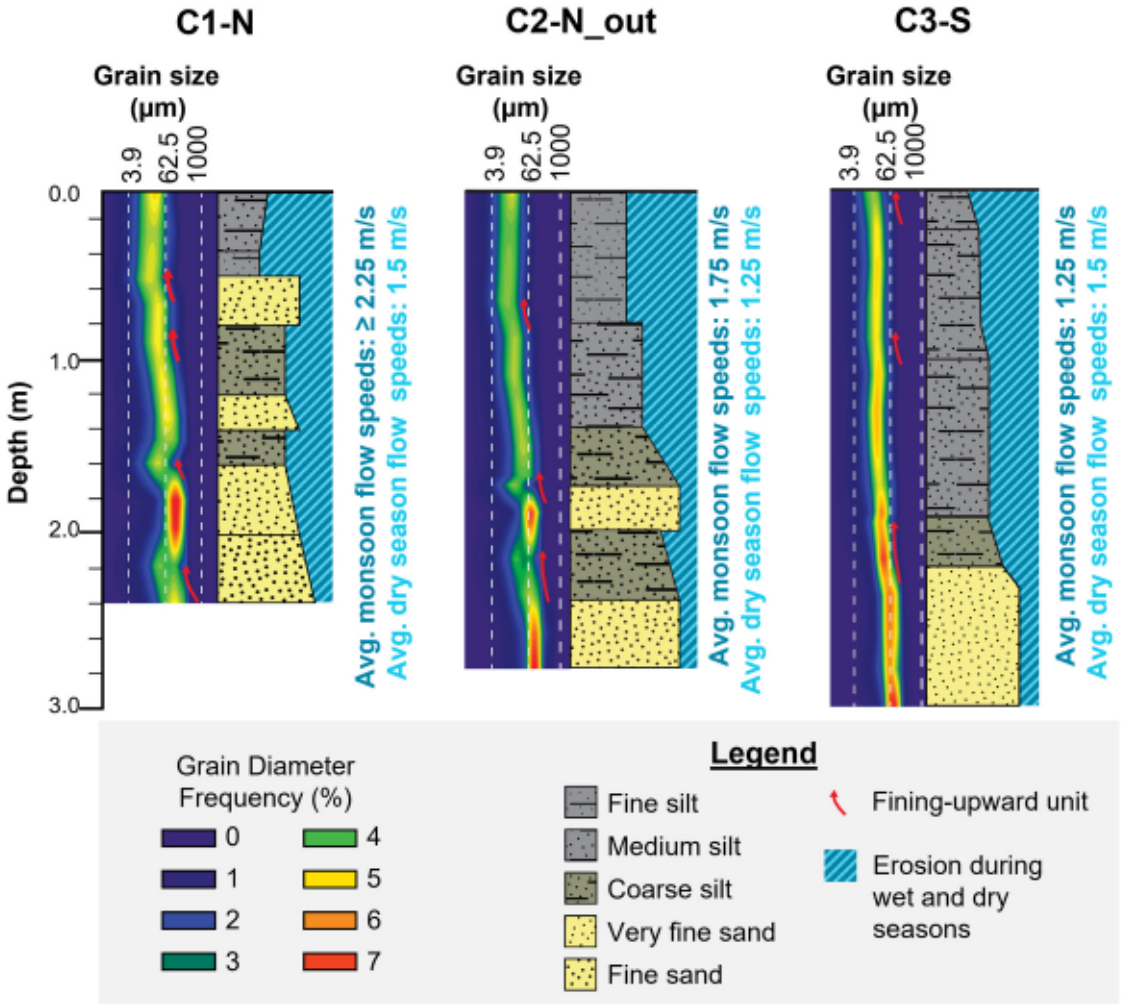

Fig. 6. Core stratigraphy at 3 representative cores for each char. Using the equations listed in Section 3.2, the erodibility of each sample for every core was assessed. For all sites, the riverbank sediments are vulnerable to erosion during both the monsoon and dry seasons. The average flow speeds for the monsoon and dry seasons for each locale are listed to the right of the cores, and the data are from (Uddin et al., 2015). Shields diagrams for each site are in Section 2 of the Supplemental Material.

Table 2
Accretion (km^2) and erosion (km^2) for all 3 sites for the 4 time intervals. Net Land Change (km^2) for 1978 to 2019 for each site was calculated, with C1 and C2 experiencing an overall loss in land while C3 experienced overall gain in land. The Total Erosion column lists the amount of land within the 225 km^2 sites that experienced erosion from 1978 to 2019. Some of the eroded land accreted again by 2019, and some of the eroded land remains water.

		Land Change (km^2)					
Site	Type of Land Change	1978 to 1991	1991 to 2001	2001 to 2010	2010 to 2019	Net Land Change (km^2)	Total Erosion (km^2)
C1	Accretion	13.7	11.7	11.6	21.0	-3.3	61.2
	Erosion	18.7	14.9	18.0	9.6		
C2	Accretion	25.9	20.5	13.2	22.9	-2.5	84.9
	Erosion	22.5	19.1	22.7	20.6		
C3	Accretion	14.6	4.1	11.0	8.6	2.2	36.0
	Erosion	12.1	9.5	7.9	6.5		

5. Discussion

5.1. Morphological and sedimentological changes of chars along the FTTZ in the Lower Meghna and Tentulia Rivers

The entirety of the Lower Meghna River, from its confluence near Chandpur to its mouth at the Bay of Bengal, is in the FTTZ Zone, as both fluvial and tidal processes shape the landscape. It is characterized by a network of chars spaced throughout its three distributary channels the Tentulia to the west, the Shahbazpur in the central region, and the Hatia to the east. The FTTZ zone not only migrates within individual distributary channels due to seasonal fluvial discharge but also across the estuary, as each channel has distinct fluvial and tidal conditions (Ahmed and Louters, 1997; Sokolewicz et al., 2008; Alam, 2014). This project focuses on chars along the upper LMR and Tentulia Channel as their population densities can exceed 1000 people per km^2 (Becker et al., 2020). Thus, while this study provides insight into char evolution and riverbank stability along the FTTZ zone of the western LMR, the results are not longitudinally applicable to the central and eastern LMR. Given the larger magnitudes of seasonal fluvial discharge and tidal influence in the Shahbazpur and Hatia channels (Ahmed and Louters, 1997; Alam, 2014), the transition zone of the FTTZ will cover a larger area (longitudinally speaking). With greater flow speeds (Alam, 2014; Uddin et al., 2015) and grain sizes (Ali et al., 2007), erosion and therefore char vulnerability in the central and eastern LMR is more widespread than the western LMR. Overall, this study highlights three geomorphological trends among chars in the western LMR FTTZ: (1) char riverbank erosion decreases downstream, (2) average char elevation decreases downstream, and (3) monsoonal flooding is the main driver of sediment and elevation dynamics in the upper LMR while tidal processes control morphodynamics in the lower Tentulia Channel.

5.1.1. Land change along the FTTZ a 2-dimensional analysis

The GBM delta has been prograding over the last 9 millennia, with 30 % of its annual sediment budget being stored in the floodplain, 40 % being deposited on the prograding delta clinothem, and the remaining 30 % being shunted into the Deep Bengal Basin via the Swatch of No Ground canyon (Goodbred and Kuehl, 1999; Rogers et al., 2013). This deltaic advancement is still observed today in the Meghna Estuary, with most accretion occurring in the eastern regions (Akhter and Mahmud, 2007; Sarwar and Woodroffe, 2013; Alam, 2014; Brammer, 2014; Roy et al., 2021). Previously calculated annual accretion rates for the entire Meghna Estuary range from 4.4 km^2 for the late 19th and early 20th centuries (Allison, 1998a) to 18.8 km^2 (Ahmed and Louters, 1997), 19.6 km^2 (Brammer, 2014), and 39.4 km^2 (Mikhailov and Dotsenko, 2007) for the past 40 years. The uptick in accretion for the latter part of the 20th century is commonly attributed to an increase in the Brahmaputra-Jamuna s sediment load, resulting from the 1950 Assam Earthquake (Sarker and Thorne, 2006; Brammer, 2014; Paszkowski et al., 2021). We calculate that for the western LMR (including the Tentulia Channel as well as the upstream LMR prior to its bifurcation), there was a net land gain of ~192 km^2 from 1978 to 2019, which is an annual accretion rate of 4.7 km^2/year (Table 1; Fig. 2). While the GBM is prograding and experiencing net accretion, erosion is simultaneously occurring and is observed as lateral migration in the land change analyses (Figs. 2, 3). Approximately 70 % of the total erosion occurred 50 km downstream of the LMR confluence (between sites C1 and C2) while ~57 % of the total land gain occurred near the Tentulia mouth, downstream of C3 (Fig. 2, Table 1). Therefore, the upstream portion of the FTTZ (where fluvial processes dominate) is generally erosional, while the downstream (more tidally influenced) region favors accretion (Fig. 2), which has been documented by previous authors in this delta (Inman, 2009; Jarriel et al., 2020). However, this study provides a more detailed analysis of land change by providing 5 land change classifications as opposed to the binary classifications for the 3 study sites as well as quantifying land change on the decadal scale dating back to 1978 (Figs. 2, 3).

Calculating the net accretion/erosion rates for endmember years is a quick and efficient way to assess overall land change, but the true mobility of chars and the prevailing hydrological processes are underrepresented. We addressed this issue in two ways: (1) we compared imagery on a decadal scale, not just the endmember years, to get a more thorough understanding of the timing of erosion and accretion within the FTTZ; (2) we chose three representative chars spaced along the FTTZ for more intensive land change analyses Char 1 (C1) which is fluvial-dominated but tidally influenced with a tidal range of 0.6 m, Char 2 (C2) which is still fluvial-dominated but more tidally influenced with a tidal range of 1.5 m, and Char 3 (C3) which is tidal- dominated but fluvially influenced with a tidal range of 1.7 m. When comparing end member years, the net land change for all 3 sites was 10 %. However, after tracing and analyzing shorelines on a decadal scale, the composite shoreline change was much larger, with a cumulative land loss of 182.1 km^2 between the three sites (Fig. 3; Table 2). The site with the most land change was C2, with ~85 km^2 of the land being eroded from 1978 to 2019. So, while a net land loss of 2.5 km^2 for C2 may not appear significant, in reality, over 37 % of the area experienced riverbank erosion at some point (Fig. 3). By comparison, C3, which is ~30 km downstream of C2, experienced less than half that erosion 36.0 km^2. By combining

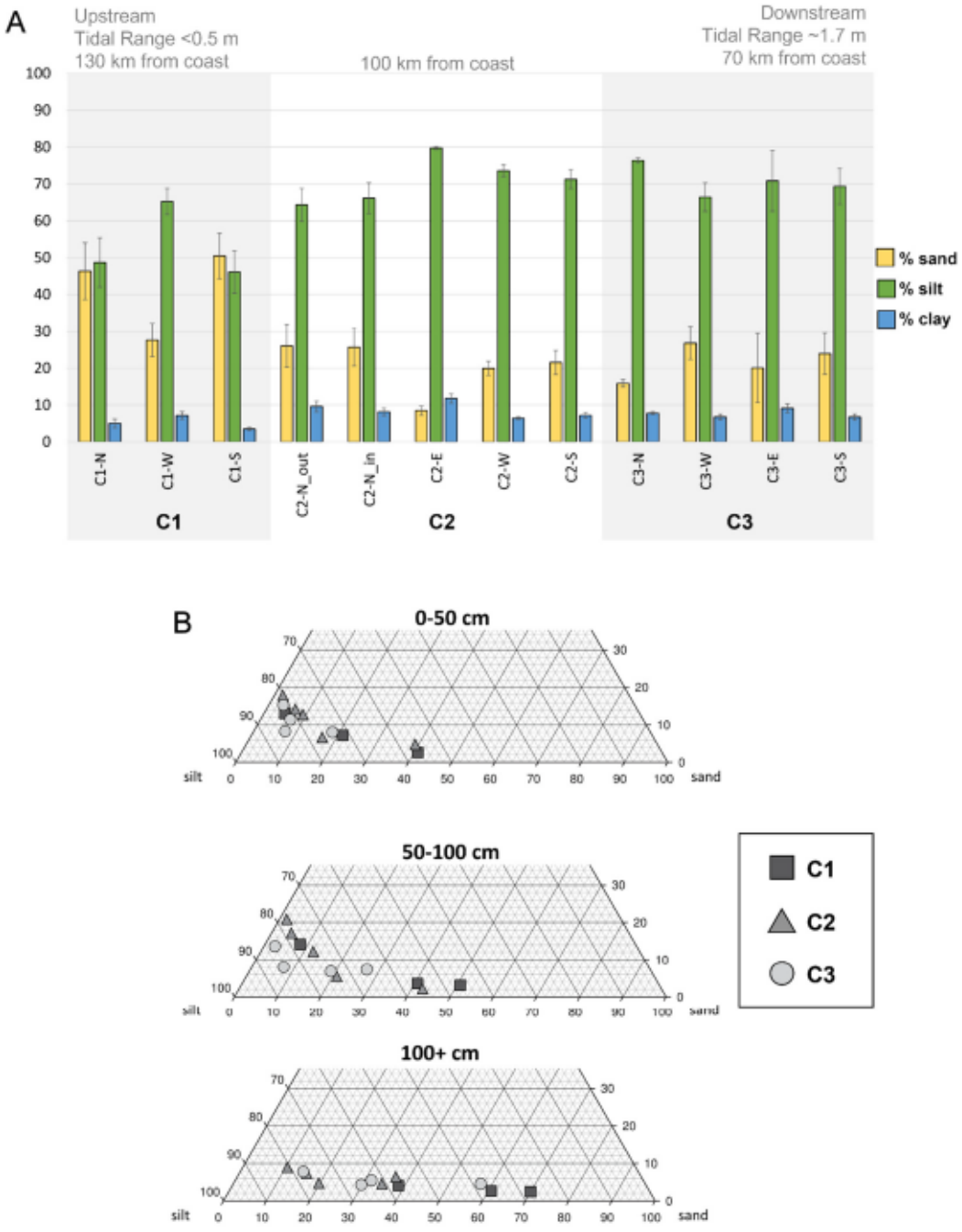

Fig. 7. Grain size distribution by (A) Hydrologic Regime and (B) Depth and (C) Site. Sites labeled with "(in)" are interior sites that are not proximal to the char shoreline. The sites are in order from the northern most sites near the confluence of the Padma and Meghna Rivers to the southernmost sites, proximal to the Bay of Bengal. As a general rule, sand decreases with proximity to the Bay of Bengal (from 50 to 25 %; A) and increases with depth (from 15 to 45 %; B). Site C1 is the sandiest of the three chars (A). Clay percentages show a small increase (<5 %; from 5 to 8 %) with respect to distance downstream and a small decrease (<10 %; from 11 to 6 %) with increasing depth. There was no discernible relationship between silt and depth (B), but there was an increase of ~34 % silt from Char 1 to Char 2 (from 53 to 71 %; A). Chars 2 and 3 had comparable amounts of silt and sand. (C) is a boxplot showing the distribution of median grain sizes between the 3 chars. There is an observable downstream fining of sediments from C1 to C2 from 63 to 34 µm.

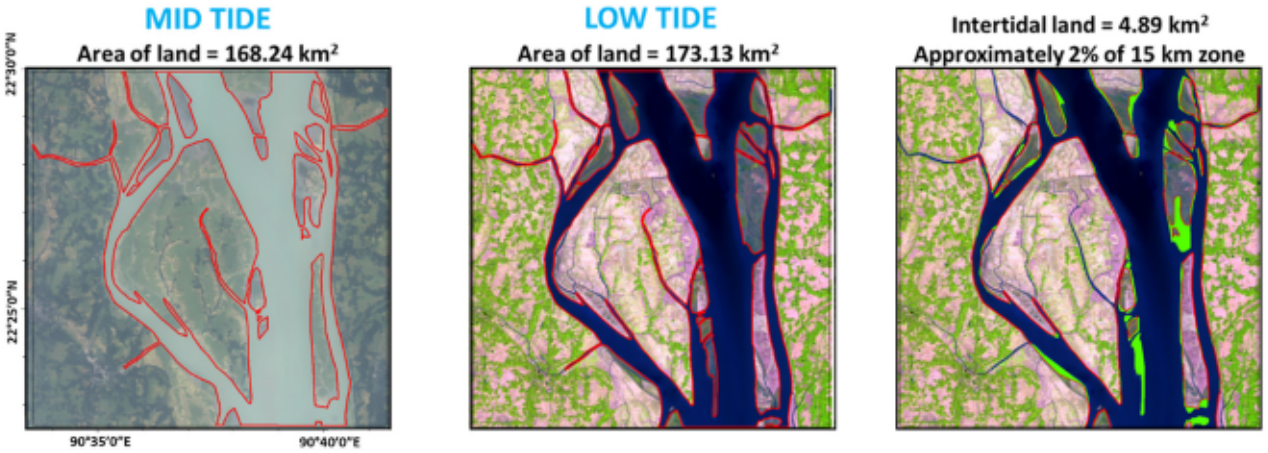

Fig. 8. Site C3 ("Box H") with a 15 km square buffer (225 km^2). Shoreline analyses was conducted for two images from 2019 – one captured at midtide and the other at low time. During midtide, ~5 km^2 of intertidal land is unaccounted for.

the binary classification with the detailed classifications, we can see that even though C2 experienced more erosion than C1, the overall trend along the FTTZ reveals a decrease in erosion (and therefore an increase in char stability) in the downstream direction. To put the total erosion into perspective from a sociological standpoint, the chars have population densities near or exceeding 1000 persons/km^2, meaning potentially 182,100 people (182.1 km^2 × 1000 persons/km^2) were affected by riverbank erosion over the past 40 years just within the three study sites (Becker et al., 2020).

It's also worth noting that even though the LMR has the 3rd largest water discharge worldwide, the GBM delta is considered to be tide-dominated, with tidal ranges increasing eastward in the Meghna Estuary (Barua, 1990; Ahmed and Louters, 1997; Allison, 1998b; Alam, 2014; Wilson and Goodbred, 2015; Hoitink et al., 2017; Gugliotta and Saito, 2019). Previous studies of shoreline erosion and accretion within the GBM delta typically utilize photo imagery collected in the dry seasons (the cloud cover is too extensive during the wet seasons for clear images) remarking either that the water levels are similar or there are uncertainties pertaining to the tidal fluctuations (Brammer, 2014; Crawford et al., 2020; Jarriel et al., 2020; Anwar and Rahman, 2021). However, analyzing imagery taken at different tide stages or at high to mid tide stages can lead to significant inaccuracies when assessing land change as intertidal land will not be visible except at low tide. For example, two images from C3 for 2019 were compared – one image was captured mid-tide while the other was from low tide; when comparing the two shorelines, nearly 5 km^2 of intertidal land was not visible in the mid-tide image (Fig. 8). Intertidal lands play a large role in coastal dynamics as they affect local hydrodynamics (Klein, 1985; Le Hir et al., 2000; Pritchard et al., 2002) and are often sites for land reclamation (Healy and Hickey, 2002; Wang et al., 2012). Thus, we show here it is critical to ensure imagery was captured at low tide when performing remote sensing analyses of meso- or macro-tidal coastal regions, such as the GBM delta (*this study*; Sarwar and Woodroffe, 2013; Mahmood et al., 2020; Roy et al., 2021).

5.1.2. Sedimentology and flow regimes – implications for char stability in the downstream FTTZ

Two key findings emerged from the data – (1) grain sizes fine downstream from the LMR to the Tentulia Channel (Fig. 7A, C) and (2) char riverbank erosion decreases downstream in the FTTZ as shown by the binary land change analyses (Fig. 2). The decrease in grain size was most apparent when comparing C1 to C2. The large difference in grain size between the char near the LMR confluence and the chars in the Tentulia can be attributed to mass extraction of sediments near the Tentulia head due to reduced fluvial current velocities; there far less reduction in velocity in the mainstem LMR, as evidenced by larger grain sizes (63–100 μm) at locations that are along the same latitude as C2 and C3 (Ali et al., 2007). Site C1 is dominated by fluvial processes, with high discharges (>100,000 m^3/s) and flow velocities (>1.5 m/s) during the monsoon season (Sokolewicz et al., 2008; Mahmud et al., 2017). The Tentulia River receives only a fraction (7 %) of the flow from the LMR during the monsoon, with much lower monsoon discharges (~20,000 m^3/s) and associated velocities (1.0–1.5 m/s) (Ahmed and Louters, 1997; Alam, 2014).

Even though the Tentulia chars have average grain sizes of ~40 μm (medium silt), which implies cohesive substrates, sand content increases with depth (Fig. 7B,C). With the significant portion of sand at depths >1 m, the chars are vulnerable to erosion through bank undercutting; that is, as the deeper, sandier layers are eroded, the overhanging upper layers collapse due to their weight. While sand content can have implications for char mobility as sand is more erodible than cohesive silts and clays (Soulsby, 1997), hydrodynamic conditions appear to play a more dominant role here. The stratigraphy around C2 and C3 have similar sediment character and grain sizes, leading one to expect comparable riverbank erosion (Fig. 7A, B, C; Fig. S4). However, C2 has much higher lateral migration (Fig. 3, Table 2). Therefore, the most likely explanation for the higher stability of C3 is its greater tidal influence – which both attenuates fluvial flow during flood tides and reduces the duration of maximum flow speeds as the velocities wax and wane depending on the tide stage (Rossi et al., 2016; Hoitink et al., 2017; Gugliotta and Saito, 2019; Iwantoro et al., 2022). C2 is ~100 km from the LMR mouth, with a tidal range of 1.5 m, and average flow velocities of 1.5–1.75 m/s during the monsoon, and C3 is ~70 km inland from the LMR mouth, with an average tidal range of 1.7 m and average flow velocities of 1.0–1.25 m/s during the monsoon (Ahmed and Louters, 1997; Alam, 2014; Uddin et al., 2014; Bricheno et al., 2016, *this study*). During the dry season, C3 has flow speeds ~1.5 m/s, which could erode all cohesive and non-cohesive sediments to depths of ~3 m. However, as C3 is tide-dominated, the duration of maximum flow speeds is limited, with flood stages lasting ~5.5 h and ebb stages lasting ~6.5 h in the Tentulia River (*this study*). Therefore, while maximum flow speeds at both C2 and C3 are great enough to erode all sediments to depths of ~3 m, C3 is more stable as the duration of its maximum flow speeds is controlled by tidal, not fluvial processes.

5.1.3. Incorporating elevation data – a 3-dimensional analysis of the FTTZ

Creating land change maps from aerial imagery is useful for predicting riverbank erosion but assessing flood vulnerability requires water surface and land surface elevation data. Recent large-scale elevation data of the GBM is severely lacking, with most studies using the Shuttle Radar Topography Mission (SRTM) Digital Elevation Model (DEM) taken in 2000. As evidenced through geospatial shoreline

Table 3
Elevation data for all survey sites, including the number of XYZ data points measured and the type of shoreline (accretionary vs erosional). There is a general decrease in average elevation with proximity to the Bay of Bengal. The only exception is C3-S, which has an average elevation of 2.3 m relative to EGM 96, making it higher than the average elevations at sites C2-S, C3-N, and C3-W. N north, S south, E east, W west.

Site			Coastal DEM v2.1 (2000; rel to EGM 96)		Leica RTK; this study (data from 2019; rel. to EGM 96)				Change in Elev. (m; 2000 to 2019)	Type of shoreline (2019)	Approx. age (years)
			Sample size (pixels)	Avg elev. (m)	Sample size (XYZ points)	Avg elev. (m)	Min. elev. (m)	Max. elev. (m)			
C1	N	10	4.5	0.5	568	4.9 0.8	2.4	5.7	0.4	Erosional	13
C1	S[a]	n/a	MSL		453	3.0 0.6	2.0	5.5	n/a	Accretionary	2
C2	N[b]	7	2.5	0.1	327	2.5 0.5	2.7	3.4	0	Erosional	41
C2	E[c]	4	3.4	0.1	190	3.1 0.1	2.9	3.0	0.3	Erosional	41
C2	S[d]	6	1.8	0.6	701	2.2 0.4	0.1	3.0	0.4	Accretionary	26
C3	N	6	2.2	0.1	335	2.0 0.1	1.1	2.1	0.2	Erosional	41
C3	W	6	1.4	0.4	522	1.4 0.3	0.0	1.8	0	Accretionary	18
C3	S	7	2.4	0.2	490	2.3 0.1	0.5	2.9	0.1	Erosional	41

[a] C1-S has an average elevation of 3.0, but it was intertidal in 2019, as the measured MSL was 3.5 m (rel to EGM 96).
[b] C2-N and C2-N(in) are adjacent to each other, thus the elevation surveys are combined.
[c] The elevation for C2-East is potentially skewed higher for the DEM elevation due to extensive tree canopy.
[d] Much of C2-S was intertidal, with elevations below the local MSL of 1.63 m (rel to EGM 96).

analyses from this study (which utilized Coastal DEM2.1v), chars in the LMR are highly mobile, and can have radically different shorelines in the span of 20 years (Fig. 3; Table 2). By incorporating new, small-scale elevation survey data with CoastalDEM data and land change analyses, we elucidate flood vulnerabilities of chars in the western LMR.

Using recent elevation data in combination with CoastalDEM 2.1v, we note that average char elevation decreases downstream, giving the LMR an overall slope of 2.1 10 ^{5}. Both SRTM data and elevation surveys from this study are referenced to EGM 96, which presents a unique challenge when assessing flood vulnerability as tide and water level data in Bangladesh is referenced to either Public Works Datum (PWD) or a local Chart Datum (CD). Neither datums have a clearly defined relationship to EGM 96. Therefore, when collecting water pressure data in the field, we measured the water surface elevations with the Leica RTK to have all three datasets referenced to EGM 96.

Having the surface and water elevation data in the same geoid allows for flood risk assessments, but it also sheds light on the shift in hydrologic regimes along the FTTZ. Three key findings illustrated in Fig. 4 are as follows: (1) char elevation decreases downstream, (2) tidal range increases downstream, and (3) elevation dynamics at C1 are controlled by fluvial processes while elevation dynamics at C3 are controlled by tidal processes. C2 lies within this continuum, with both processes significantly contributing to the morphology. The third finding, which is potentially the most important with regards to flood vulnerability and land change, is based on floodplain hydrodynamics. In a floodplain setting, the surrounding landscape aggrades to the highest flood extent. For fluvial settings, this is controlled by the river flood stages (Törnqvist and Bridge, 2002; Shen et al., 2015), and in tidal settings, floodplains aggrade to the tidal mean high water (MHW) (Kirwan and Guntenspergen, 2010; Bomer et al., 2020). In deltaic settings where fluvial and tidal forcings interact, parsing out the dominant hydrologic regime can be more challenging.

At Char 1, the average MHW is ~0.3 m below the char s average elevation and 1.9 m below its maximum elevation (Fig. 4, Table 3). Tide tables from Bangladesh Inland Water Transport Authority (BIWTA) reveal a 2 m difference in water levels between the dry and wet seasons for Chandpur, which is located 2 km across the LMR from C1. As C1 has a tidal range of ~0.6, it can be ascertained that the high water levels, and therefore the char elevation, is highly controlled by fluvial processes (i.e., monsoon flood water levels). At C2, average char elevations once again exceed MHW, but only by ~0.15 m. Pressure sensor data (HOBO) that was collected for a period of 1 year at C2 determine that maximum flood level was 3.5 m (rel to EGM 96) during the monsoon, the same as maximum elevations on C2 (Fig. 4). Therefore, fluvial processes still dominate at C2 as the maximum elevations align with the maximum monsoon water levels, but tidal processes appear to have more influence on char sediment dynamics as the maximum elevations for C2 are only 1.15 m above MHW (Fig. 4, Table 3). Finally, at C3, the southernmost char, the MHW is only 0.05 m above the average char elevation. Thus, the platform has aggraded to MHW, as typical of tide-dominated floodplains (Friedrichs and Perry, 2001; Kirwan and Guntenspergen, 2010). BIWTA tide tables reveal that water levels increase by 0.5 1.0 m during the monsoon, making maximum water levels and thereby maximum char elevations ~3.0 m (rel to EGM 96).

5.2. Implications for flood risk

Flood risk in the Meghna Estuary varies by location along the FTTZ areas in the upstream, fluvial-dominated regions are most affected by monsoonal flood pulses (as reflected in the elevation dynamics shown in Fig. 4), while flood risk associated with SLR, cyclones, and storm surges increases with proximity to the coast (Sarker et al., 2003; A. S. Islam et al., 2013; M. Islam et al., 2013; Islam and Hasan, 2016; Becker et al., 2020). As evidenced by this study, char elevations in the lower ~70 km of the Tentulia channel are driven by tidal processes, aggrading to the MHW (Fig. 4). Under natural circumstances, chars and adjacent

floodplains could keep pace with RSLR (~1 cm/yr; Allison and Kepple, 2001; Rogers et al., 2013) as long as sediment delivery is unimpeded (Kirwan and Guntenspergen, 2010; Brammer, 2014; Bomer et al., 2020). However, many coastal chars are embanked (i.e., poldered) as a means of protection from storm surges and salinity intrusion (Fig. 1). An unintended consequence of embankments is land loss due to sediment starvation and compaction, which leaves the embanked agricultural lands and its citizens vulnerable to flooding if an embankment should fail during a cyclone or storm surge (Auerbach et al., 2015; Bomer et al., 2020; Valentine et al., 2021). The Institute of Water Modelling (IWM) in Bangladesh predicts that by 2050, rising sea levels and increased cyclone intensities can lead to inundation depths exceeding 6 m in the mainstem LMR (Shahbazpur and Hatia Channels), ranging from 3 to 6 m for the entire Tentulia Channel, and could even exceed 1 m as far north as Chandpur; at these surge heights, all coastal polders and embankments are vulnerable to overtopping (Dasgupta et al., 2010). Not all chars along the Tentulia are currently embanked, but river water salinity along the Tentulia and LMR are projected to increase to levels that will result in 26 50 % agricultural yield reduction in the next 30 years (Clarke et al., 2015; Dasgupta et al., 2015). As a result, more chars along the FTTZ will most likely be embanked as a means to protect arable land (Haque et al., 2018; Haque et al., 2019), effectively cutting off water and sediment supply to the char interiors. Thus, chars in the downstream, tidally-dominated region of the FTTZ will face major flooding issues in the future if they are embanked as the platforms will no longer be able to aggrade with rising sea levels.

6. Conclusions

Here we use a multi-faceted approach to better constrain the fluvial and tidal processes within the Fluvial Tidal Transition Zone (FTTZ) of the lower Ganges Brahmaputra delta, specifically within the western Lower Meghna River (and Tentulia Channel). Overall, the FTTZ has been gaining land at a rate of 4.7 km^2/yr over the last 40 years, with 70 % of land loss occurring within 50 km of the LMR confluence (~100 km inland from coast) and 50 % of land gain occurring in the Tentulia Channel within 50 km of the coast. Further land change analyses highlight that net land gain/loss estimates gloss over the overall land change and vulnerability of chars to riverbank erosion. For example, focus areas investigated here show a combined 182 km^2 of land loss, with C2 (100 km from coast, between the fluvial-dominated and tidal-dominated regions of the FTTZ) experiencing most riverbank erosion. Sedimentological data revealed a general downstream fining in grain size, especially from the mainstem LMR to the Tentulia channel, which receives 25 % of the LMR s flow throughout the year. There was evidence of slight downstream fining from C2 to C3, but the char sedimentology was so similar that the stability of C3 is attributed to increased tidal influence. The flood current of the tides attenuates fluvial flow, and the duration of maximum flow speeds is limited to the apices of flood and ebb stages, with near-zero flow speeds occurring during slack tides. Land change analyses, sedimentology, and elevation surveys were combined to provide a 3-Dimenisional assessment of the sediment dynamics along the FTTZ. Fluvial processes, namely riverine monsoonal flooding, controls channel erosion and morphology in the upper LMR (near focus area C1). Fluvial processes still appear to be the dominating process near the head of the Tentulia Channel, but elevation and water level data show an increase in tidal influence. The tipping point appears to be at or just downstream of focus area C3 (~70 km from the coast), where (1) elevation dynamics start to mirror tidal MHW rather than riverine monsoonal flooding and (2) land change analyses show a reduction in riverbank erosion. While the fluvial-dominated chars are vulnerable to riverbank erosion from increased fluvial discharge during the monsoon season, tidal-dominated chars in the FTTZ are most vulnerable to flooding associated with cyclones and SLR, with predicted inundation depths from cyclone storm surges exceeding 3 m by 2050 (Dasgupta et al., 2010). With approximately 3000 km^2 of charland in the LMR and population densities ranging from 750 to 1000 persons/km^2, 2 3 million people living in the FTTZ from the LMR to the coast are vulnerable to the effects of climate change (Sarker et al., 2003; Syvitski et al., 2009; Dasgupta et al., 2015; Paszkowski et al., 2021).

Declaration of competing interest

The authors declare that they have no known competing financial interests or personal relationships that could have appeared to influence the work reported in this paper.

Data availability

Datasets associated with this project are provided in the Supplementary Material. Any associated data not included in the Supplementary Material will be archived with co-author C.A. Wilson and housed at Louisiana State University. As per NSF guidelines, this material will be made publicly accessible, and access and permission to use this associated data can be provided after a formal written request is received and accepted.

Acknowledgements

We wish to thank the following for assistance in the field: Hafizur Rahaman, Shakir Ahmed, Arifur Rahman, Abdullah Al Nahian, and Zahidul Shawon. We also thank Grant Lopez, Michael Piorkowski, and Sophie Vincent for assistance with laboratory work. This study was funded by the National Science Foundation, Award 1716909 (CNH-L).

Appendix A. Supplementary data

Supplementary data to this article can be found online at https://doi.org/10.1016/j.geomorph.2023.108692.

References

Ahmed, S., Louters, T., 1997. In: Meghna Estuary Study: Technical Note: Residual Tidal Volume and Sediment Transport Patterns in the Lower Meghna Estuary During Premonsoon and Postmonsoon - An Analysis of Available Land Reclamation Projects Data Collected During 1986-94, p. 28.

Akhter, F., Mahmud, F., 2007. A Study on Erosion and Accretion of the Main Islands in the Meghna Estuary. Dept. of Water Resources Engineering, BUET, Dhaka. B. Sc. Engg. Thesis.

Alam, M., 1996. Subsidence of the Ganges-Brahmaputra Delta of Bangladesh and associated drainage, sedimentation and salinity problems. Available at:. In: Coastal Systems and Continental Margins, 2, pp. 169 192 http://libezp.lib.lsu.edu/login?url http://search.ebscohost.com/login.aspx?direct true&db geh&AN 1 997-006545&site ehost-live&scope site.

Alam, R., 2014. Characteristics of hydrodynamic processes in the Meghna estuary due to dynamic whirl action. IOSR J. Eng. 4 (6), 39 50. https://doi.org/10.9790/3021-04633950.

Ali, A., Mynett, A.E., Azam, M.H., 2007. Sediment Dynamics in the Meghna Estuary, Bangladesh: a Model Study. J. Waterw. Port Coast. Ocean Eng. 133 (4), 255 263. https://doi.org/10.1061/(asce)0733-950x(2007)133:4(255).

Allison, M.A., 1998a. Geologic framework and environmental status of the Ganges-Brahmaputra delta. J. Coast. Res. 14 (3), 826 836.

Allison, M.A., 1998b. Historical changes in the Ganges-Brahmaputra delta front. J. Coast. Res. 14 (4), 1269 1275.

Allison, M.A., Kepple, E., 2001. Modern sediment supply to the lower delta plain of the Ganges-Brahmaputra River in Bangladesh. Geo-Mar. Lett. 21 (2), 66 74. https://doi.org/10.1007/s003670100069.

Anwar, M.S., Rahman, K., 2021. The Spatiotemporal Shore Morphological changes at East Bhola Island in Meghna Estuary of Bangladesh s Central Coast. Reg. Stud. Mar. Sci. 47 https://doi.org/10.1016/j.rsma.2021.101937.

Arun, P.V., 2013. A comparative analysis of different DEM interpolation methods. Egyptian J. Remote Sens. Space Sci. 16 (2), 133 139. https://doi.org/10.1016/j.ejrs.2013.09.001.

Ashworth, P.J., et al., 2000. Morphological evolution and dynamics of a large, sand braid-bar, Jamuna River, Bangladesh. Sedimentology 47 (3), 533 555. https://doi.org/10.1046/j.1365-3091.2000.00305.x.

Auerbach, L.W., et al., 2015. Flood risk of natural and embanked landscapes on the Ganges-Brahmaputra tidal delta plain. Nat. Clim. Chang. 5 (2), 153 157. https://doi.org/10.1038/nclimate2472.

Barros, M.de L.C., et al., 2011. A water flow pattern analysis of Guajará Bay: Amazon Estuary-Brazil. J. Braz. Soc. Mech. Sci. Eng. 33, 79 85.

Barua, D.K., 1990. Suspended sediment movement in the estuary of the Ganges-Brahmaputra-Meghna river system. Mar. Geol. 91 (3), 243 253. https://doi.org/10.1016/0025-3227(90)90039-M.
Becker, M., et al., 2020. Water level changes, subsidence, and sea level rise in the Ganges-Brahmaputra-Meghna delta. Proc. Natl. Acad. Sci. U. S. A. 117 (4), 1867 1876. https://doi.org/10.1073/pnas.1912921117.
Best, J.L., et al., 2003. Three-dimensional sedimentary architecture of a large, mid-channel sand braid bar, Jamuna River, Bangladesh. J. Sediment. Res. 73 (4), 516 530.
Best, J.L., et al., 2007. The Brahmaputra-Jamuna River, Bangladesh. In: Large Rivers: Geomorphology and Management, pp. 395 430.
Bomer, E.J., et al., 2020. Surface elevation and sedimentation dynamics in the Ganges-Brahmaputra tidal delta plain, Bangladesh: evidence for mangrove adaptation to human-induced tidal amplification. Catena 187 (September 2019), 104312. https://doi.org/10.1016/j.catena.2019.104312.
Bomer, E.J., Wilson, C.A., Datta, D.K., 2019. An integrated approach for constraining depositional zones in a tide-influenced river: insights from the Gorai River, Southwest Bangladesh. Water 11 (10), 2047.
Brammer, H., 2014. Bangladesh s dynamic coastal regions and sea-level rise. Clim. Risk Manag. 1, 51 62. https://doi.org/10.1016/j.crm.2013.10.001.
Bricheno, L.M., Wolf, J., Islam, S., 2016. Tidal intrusion within a mega delta: an unstructured grid modelling approach. Estuar. Coast. Shelf Sci. 182, 12 26. https://doi.org/10.1016/j.ecss.2016.09.014.
Clarke, D., et al., 2015. Projections of on-farm salinity in coastal Bangladesh. Environ. Sci. Process. Impacts 17 (6), 1127 1136. https://doi.org/10.1039/c4em00682h.
Crawford, T.W., et al., 2020. Coastal erosion and human perceptions of revetment protection in the Lower Meghna estuary of Bangladesh. Remote Sens. 12 (18), 1 24. https://doi.org/10.3390/RS12183108.
Dalrymple, R.W., Choi, K., 2007. Morphologic and facies trends through the fluvial-marine transition in tide-dominated depositional systems: a schematic framework for environmental and sequence-stratigraphic interpretation. Earth Sci. Rev. 81 (3 4), 135 174. https://doi.org/10.1016/j.earscirev.2006.10.002.
Dasgupta, S., et al., 2010. Vulnerability of bangladesh to cyclones in a changing climate: potential damages and adaptation cost. In: World Bank Policy Research Working Paper, 5280.
Dasgupta, S., et al., 2015. Climate change and soil salinity: the case of coastal Bangladesh. Ambio 44 (8), 815 826. https://doi.org/10.1007/s13280-015-0681-5.
Elahi, M.W.E., et al., 2020. Influence of seasonal river discharge on tidal propagation in the Ganges-Brahmaputra-Meghna Delta, Bangladesh. J. Geophys. Res. Oceans 125 (11). https://doi.org/10.1029/2020JC016417.
Friedrichs, C.T., Perry, J.E., 2001. Tidal salt marsh morphodynamics: a synthesis. J. Coast. Res. 7 37.
Goodbred, S.L., Kuehl, S.A., 1999. Holocene and modern sediment budgets for the Ganges-Brahmaputra river system: evidence for highstand dispersal to flood-plain, shelf, and deep-sea depocenters. Geology 27 (6), 559 562. https://doi.org/10.1130/0091-7613(1999)027 0559:HAMSBF 2.3.CO;2.
Gugliotta, M., Saito, Y., 2019. Matching trends in channel width, sinuosity, and depth along the fluvial to marine transition zone of tide-dominated river deltas: the need for a revision of depositional and hydraulic models. Earth Sci. Rev. 191, 93 113.
Hale, R., et al., 2019. Observations and scaling of tidal mass transport across the lower Ganges-Brahmaputra delta plain: Implications for delta management and sustainability. Earth Surf. Dyn. 7 (1), 231 245. https://doi.org/10.5194/esurf-7-231-2019.
Haque, A., et al., 2019. Inundation due to future climate and proposed interventions. In: Rahman, M., et al. (Eds.), Integrated Assessment for the Bangladesh Delta Plan 2100: Analysis of selected interventions. BUET-Southampton University-GED. Planning Commission, People s Republic of Bangladesh, pp. 13 26.
Haque, A., Kay, S., Nicholls, R.J., 2018. Present and future fluvial, tidal, and storm surge flooding in coastal Bangladesh. In: Nicholls, R.J., et al. (Eds.), Ecosystem Services for Well-being in Deltas: Integrated Assessment for Policy Analysis. Springer Nature, pp. 293 314.
Harris, P.T., et al., 2004. Sediment transport in distributary channels and its export to the pro-deltaic environment in a tidally dominated delta: Fly River, Papua New Guinea. Cont. Shelf Res. 24 (19), 2431 2454. https://doi.org/10.1016/j.csr.2004.07.017.
Healy, M.G., Hickey, K.R., 2002. Historic land reclamation in the intertidal wetlands of the Shannon estuary, western Ireland. Journal of Coastal Research 36 (10036), 365 373.
Le Hir, P., et al., 2000. Characterization of intertidal flat hydrodynamics. Cont. Shelf Res. 20 (12 13), 1433 1459.
Hoitink, A.J.F., et al., 2017. Tidal controls on river delta morphology. Nat. Geosci. 10 (9), 637 645. https://doi.org/10.1038/ngeo3000.
Inman, M., 2009. Where warming hits hard. Nat. Clim. Chang. 1 (902), 18 21.
Islam, A.S., et al., 2013. Assessment of Capabilities, Needs of Communities, Opportunities and Limitations of Weather Forecasting for Coastal Regions of Bangladesh. WorldFish.
Islam, M., et al., 2013. Coping Techniques of local people to Flood and River erosion in Char areas of Bangladesh. J. Environ. Sci. Nat. Resour. 5 (2), 251 261. https://doi.org/10.3329/jesnr.v5i2.14827.
Islam, M.R., Hasan, M., 2016. Climate-induced human displacement: a case study of Cyclone Aila in the south-west coastal region of Bangladesh. Nat. Hazards. https://doi.org/10.1007/s11069-015-2119-6.
Iwantoro, A.P., van der Vegt, M., Kleinhans, M.G., 2022. Stability and asymmetry of tide-influenced river bifurcations. J. Geophys. Res. Earth Surf. 127 (6), e2021JF006282.
Jarriel, T., et al., 2020. System wide channel network analysis reveals hotspots of morphological change in anthropogenically modified regions of the Ganges Delta. Sci. Rep. 10 (1), 1 12.
Kale, V.S., 2003. Geomorphic effects of monsoon floods on Indian rivers. Nat. Hazards 28 (1), 65 84. https://doi.org/10.1023/A:1021121815395.
Khan, N.I., Islam, A., 2003. Quantification of erosion patterns in the Brahmaputra-Jamuna River using geographical information system and remote sensing techniques. Hydrol. Process. 17 (5), 959 966. https://doi.org/10.1002/hyp.1173.
Kirwan, M.L., Guntenspergen, G.R., 2010. Influence of tidal range on the stability of coastal marshland. J. Geophys. Res. Earth Surf. 115 (F2), 1 11. https://doi.org/10.1029/2009jf001400.
Klein, G., 1985. Intertidal flats and intertidal sand bodies. In: Coastal Sedimentary Environments. Springer, pp. 187 224.
Kulp, S.A., Strauss, B.H., 2019. New elevation data triple estimates of global vulnerability to sea-level rise and coastal flooding. Nat. Commun. 10 (1), 1 12.
Kulp, S.A., Strauss, B.H., 2021. CoastalDEM v2. 1: A High-accuracy and High-resolution Global Coastal Elevation Model Trained on ICESat-2 Satellite Lidar.
Mahmood, R., et al., 2020. Coastal vulnerability assessment of Meghna estuary of Bangladesh using integrated geospatial techniques. Int. J. Disas. Risk Reduc. 42, 101374 https://doi.org/10.1016/j.ijdrr.2019.101374.
Mahmud, I.H., et al., 2017. A study on seasonal variation of hydrodynamic parameters of Padma River. Available at: Journal of Modern Science and Technology 5 (1), 1 10 http://jmstpapers.com/static/documents/September/2017/Issue/1.Zishan.pdf.
Mikhailov, V.N., Dotsenko, M.A., 2007. Processes of delta formation in the mouth area of the Ganges and Brahmaputra rivers. Water Resour. 34 (4), 385 400. https://doi.org/10.1134/S0097807807040033.
Neill, C., Hotopp, D., Hunter, B., 2013. In: Some Hydrotechnical Features of Padma River, Bangladesh, pp. 1 11.
Nowacki, D.J., et al., 2015. Sediment dynamics in the lower Mekong River: transition from tidal river to estuary. J. Geophys. Res. Oceans 120 (9), 6363 6383.
Oberhagemann, K., Sarker, M.H., Huque, I., 2021. The morphology of riverine chars. In: Living on the Edge. Springer, pp. 121 140.
Paszkowski, A., et al., 2021. Geomorphic change in the Ganges Brahmaputra Meghna delta. Nat. Rev. Earth Environ. 2 (11), 763 780. https://doi.org/10.1038/s43017-021-00213-4.
Pritchard, D., Hogg, A., Roberts, W., 2002. Morphological modelling of intertidal mudflats: the role of cross-shore tidal currents. Cont. Shelf Res. 22 (11 13), 1887 1895.
Rogers, K.G., Goodbred Jr., S.L., Mondal, D.R., 2013. Monsoon sedimentation on the 'abandoned tide-influenced Ganges-Brahmaputra delta plain. Estuar. Coast. Shelf Sci. 131, 297 309.
Rossi, V.M., et al., 2016. Impact of tidal currents on delta-channel deepening, stratigraphic architecture, and sediment bypass beyond the shoreline. Geology 44 (11), 927 930.
Roy, S., et al., 2021. Coastal erosion risk assessment in the dynamic estuary: the Meghna estuary case of Bangladesh coast. Int. J. Disas. Risk Reduc. 61, 102364 https://doi.org/10.1016/j.ijdrr.2021.102364.
Ruknul Ferdous, M., et al., 2018. Socio-hydrological spaces in the Jamuna River floodplain in Bangladesh. Hydrol. Earth Syst. Sci. 22 (10), 5159 5173. https://doi.org/10.5194/hess-22-5159-2018.
Sarker, M.H., et al., 2003. Rivers, charsandchar dwellers of Bangladesh. Int. J. River Basin Manag. 1 (1), 61 80.
Sarker, M.H., Thorne, C.R., 2006. Morphological response of the Brahmaputra Padma Lower Meghna river system to the Assam earthquake of 1950. In: Braided Rivers: Process, Deposits, Ecology and Management, 21, pp. 289 310.
Sarwar, M.G.M., Woodroffe, C.D., 2013. Rates of shoreline change along the coast of Bangladesh. J. Coast. Conserv. 17 (3), 515 526. https://doi.org/10.1007/s11852-013-0251-6.
Shen, Z., et al., 2015. Episodic overbank deposition as a dominant mechanism of floodplain and delta-plain aggradation. Geology 43 (10), 875 878.
Snyder, J.P., 1997. Flattening the Earth: Two Thousand Years of Map Projections. University of Chicago Press.
Sokolewicz, M., Zhang, G., Louters, T., 2008. Planform Development of the Meghna Estuary in Bangladesh.
Soulsby, R., 1997. Dynamics of Marine Sands.
Syed, Z.H., Choi, G., Byeon, S., 2018. A numerical approach to predict water levels in ungauged regions case study of the Meghna river estuary, Bangladesh. Water (Switzerland) 10 (2). https://doi.org/10.3390/w10020110.
Syvitski, J.P.M., et al., 2009. Sinking deltas due to human activities. Nat. Geosci. 2 (10), 681 686. https://doi.org/10.1038/ngeo629.
Törnqvist, T.E., Bridge, J.S., 2002. Spatial variation of overbank aggradation rate and its influence on avulsion frequency. Sedimentology 49 (5), 891 905. https://doi.org/10.1046/j.1365-3091.2002.00478.x.
Uddin, M., et al., 2014. Two dimensional hydrodynamic modelling of northern Bay of Bengal coastal waters. Comput. Water Energy Environ. Eng. 03 (04), 140 151. https://doi.org/10.4236/cweee.2014.34015.
Uddin, M.M., et al., 2015. Numerical simulation: hydro-morphology of Meghna Estuary. Int. J. Ocean Clim. Syst. 6 (4), 173 184.
Valentine, L., Wilson, C.A., Rahman, M., 2021. Floodrisk of embanked areas and potential use of dredge spoils as mitigation measures in the southwest region of the Ganges-Brahmaputra-Meghna Delta, Bangladesh. Earth Surf. Process. Landf. https://doi.org/10.1002/esp.5303.
Wang, Y.P., et al., 2012. Sediment transport over an accretional intertidal flat with influences of reclamation, Jiangsu coast, China. Marine Geology 291, 147 161.
Wilson, C.A., Goodbred, S.L., 2015. Construction and maintenance of the Ganges-Brahmaputra-Meghna delta: linking process, morphology, and stratigraphy. Annu. Rev. Mar. Sci. 7, 67 88. https://doi.org/10.1146/annurev-marine-010213-135032.